Journal of ELECTRONIC MATERIALS, Vol. 45, No. 5, 2016
DOI: 10.1007/s11664-015-4314-3

Application of Graphene Oxide-$MnFe_2O_4$ Magnetic Nanohybrids as Magnetically Separable Adsorbent for Highly Efficient Removal of Arsenic from Water

PHAM THI LAN HUONG,[1] LE THANH HUY,[1,2] VU NGOC PHAN,[1] TRAN QUANG HUY,[3] MAN HOAI NAM,[4] VU DINH LAM,[4] and ANH-TUAN LE[1,5]

1.—Department of Nanoscience and Nanotechnology, Advanced Institute for Science and Technology (AIST), Hanoi University of Science and Technology (HUST), No. 1, Dai Co Viet Street, Hai Ba Trung District, Hanoi, Vietnam. 2.—Faculty of Chemistry and Environment Technology, Hung Yen University of Technology and Education, Khoai Chau, Hung Yen, Vietnam. 3.—National Institute of Hygiene and Epidemiology (NIHE), 1-Yersin Street, Hai Ba Trung District, Hanoi, Vietnam. 4.—Institute of Materials Science, Vietnam Academy of Science and Technology (VAST), 18 Hoang Quoc Viet, Hanoi, Vietnam. 5.—e-mail: tuan.leanh1@hust.edu.vn

In this work, a functional magnetic nanohybrid consisting of manganese ferrite magnetic nanoparticles ($MnFe_2O_4$) deposited onto graphene oxide (GO) nanosheets was successfully synthesized using a modified co-precipitation method. The as-prepared GO-$MnFe_2O_4$ magnetic nanohybrids were characterized using x-ray diffraction, transmission electron microscopy, Fourier transformed infrared spectroscopy, and vibrating sample magnetometer measurements. Adsorption experiments were performed to evaluate the adsorption capacities and efficient removal of arsenic of the nanohybrid and compared with bare $MnFe_2O_4$ nanoparticles and GO nanosheets. Our obtained results reveal that the adsorption process of the nanohybrids was well fitted with a pseudo-second-order kinetic equation and a Freundlich isotherm model; the maximum adsorption capacity and removal efficiency of the nanohybrids obtained ~240.385 mg/g and 99.9% with a fast response of equilibrium adsorption time ~20 min. The larger adsorption capacity and shorter equilibrium time of the GO-$MnFe_2O_4$ nanohybrids showed better performance than that of bare $MnFe_2O_4$ nanoparticles and GO nanosheets. The advantages of reusability, magnetic separation, high removal efficiency, and quick kinetics make these nanohybrids very promising as low-cost adsorbents for fast and effective removal of arsenic from water.

Key words: Adsorption isotherm, $MnFe_2O_4$-GO magnetic nanohybrid, adsorbent, arsenic removal

INTRODUCTION

Nowadays, water pollution is a challenge facing many developing countries due to rapid development of industrialization and urbanization.[1] The pollution of heavy metal ions in groundwater causes a serious health risk to human health and ecology. Arsenic contamination of groundwater has caused a massive epidemic of arsenic poisoning worldwide, especially the arsenic poisoning found in South and South East Asia areas.[1,2] According to the World Health Organization standard, arsenic is highly toxic and has a carcinogenic element when its concentration >0.01 mg/L (10 ppb-part per billion). In Vietnam, under a survey reported in 2013 of "Human exposure to arsenic from drinking water in Vietnam", they revealed that the arsenic contamination in groundwater was found in several of Vietnam's north provinces that had an arsenic

(Received October 9, 2015; accepted December 17, 2015; published online January 4, 2016)

concentration above >10 ppb standard.[2] The contamination level of arsenic in groundwater is up to 0.05 mg/L. This high arsenic level can cause several health issues such as skin cancer and/or dermatitis. Therefore, the requirement for complete removal of arsenic from groundwater is an emerging problem for developing countries such as Vietnam.

To remove the arsenic from water, the magnetic nanoparticles of iron oxide-based materials (i.e., Fe_3O_4) or ferrite materials (MFe_2O_4, M = Ni, Mn, Zn) were proved as effective adsorbents in the removal of heavy metal ions and arsenic including arsenate As(V) and arsenite As(III).[3–5] However, these nanoparticle adsorbents showed some disadvantages such as difficulty in using in continuous flow systems due to their instability and agglomeration. To overcome this challenge, several researchers have combined magnetic nanoparticles with carbon materials.

Recently, graphene oxide (GO), an oxidation product of graphene,[6,7] has received considerable attention from the scientific community for environmental treatment applications because of their excellent adsorption properties.[8–12] The GO nanosheets are chemically synthesized graphene sheets that are modified with oxygen-containing functional groups; therefore, the GO nanosheets can be ideally used as catalyst carrier substances due to their large surface area and long-term stable dispersion. These advantages motivated us to synthesize a nanosized hybrid material for highly effective arsenic removal.

In this work, we report a new kind of magnetic nanohybrid based on the GO sheets and $MnFe_2O_4$ (MFO) manganese ferrite nanoparticles. The arsenic adsorption process of GO-MFO nanohybrid is thoroughly studied and compared with bare MFO and GO nanosheets. Our results reveal that the GO-MFO sample shows better adsorption performance of larger adsorption capacity and shorter equilibrium time than that of bare MFO nanoparticles and GO samples. The maximum adsorption capacity and removal efficiency of the nanohybrids obtain ~240.385 mg/g and 99.9% with a fast response of equilibrium adsorption time ~20 min. These exhibited excellent properties make GO-MFO nanohybrids very promising as low-cost adsorbent for fast and effective removal of arsenic from water.

EXPERIMENTAL PROCEDURES

Chemicals

Analytical-grade manganese chloride tetrahydrate ($MnCl_2{\cdot}4H_2O$, ≥ 99%), ferric chloride hexahydrate hydrogen ($FeCl_3{\cdot}6H_2O$ ≥ 99%), sodium hydroxide (NaOH), ammonium hydroxide (NH_3, 25%), potassium permanganate ($KMnO_4$, 99.9%), hydrogen peroxide (H_2O_2, 30%), sulfuric acid (H_2SO_4, 98%), hydrochloric acid (HCl, 37%), and nitric acid (HNO_3, 63%) used in this study were purchased from Shanghai Chemical Reagent Co. Ltd.

Synthesis of Graphene Oxide (GO) by the Modified Hummers Method

The GO nanosheets were synthesized from coal powder by the modified Hummers method as described previously.[13,14] Briefly, 1 g of coal powders were mixed with HNO_3 and $KMnO_4$ at a volume ratio of 1:2:1.5, respectively, and then the mixture was converted to exploited graphite (EG) under microwaves at 800 W for 1 min. In this reaction, the mixture of 2 g of EG, 8 g of $KMnO_4$, and 1 g of $NaNO_3$ was added slowly to 160 mL of 98% H_2SO_4 at 5°C in a ice-water bath and then stirred for 30 min. The ice-water bath was removed, and then the temperature was increased slowly to 45°C and continuously stirred for 2 h. Deionized water was added slowly to the mixture, which was stirred until purple fumes were inhibited. By increasing the reaction temperature to 95°C and stirring the mixture for 1 h, the resulting product of the GO nanosheets was obtained with a yellow–brown color. The GO nanosheets were then treated by H_2O_2 30% and HCl 10% solution to eliminate $KMnO_4$, MnO_2, and other metal ions that remained in the GO solution. The final GO products were purified by filtering, washing several times by ultrasonic vibration, centrifugation with deionized water, and removal of ultrafine carbon powder that was not oxidized.

Synthesis of $MnFe_2O_4$ Nanoparticles by the Co-precipitation Method

The $MnFe_2O_4$ (MFO) NPs were synthesized by a co-precipitation method. Briefly, 2.7 g (0.02 mol) $FeCl_3{\cdot}6H_2O$ and 0.99 g (0.01 mol) $MnCl_2{\cdot}4H_2O$ were dissolved in 100 mL of deionized water and stirred under air for 10 min so that the molar ratio of Mn:Fe in the solution was 1:2. Then, a 0.5 M NaOH solution was slowly added into the mixture. The color of the solution changed immediately from orange to dark brown. After that, the mixture was stirred in water bath at 80°C for a period of time. The precipitate was collected by a magnet and washed several times with deionized water before being dried at 80°C for 1 h. The main advantages of this method are short synthesis time, high crystallinity, and low cost.

Synthesis of GO-$MnFe_2O_4$ Nanohybrid by the Modified Co-precipitation Method

In the same way, the GO-$MnFe_2O_4$ (GO-MFO) nanohybrids were synthesized by a modified co-precipitation method. The $FeCl_3{\cdot}6H_2O$ and $MnCl_2{\cdot}4H_2O$ were dissolved in deionized water with a molar ratio of Mn:Fe in solution at 1:2. The resulting mixture was mixed with GO suspension (0.6 mg/mL) while stirring for 30 min. The solution

was then constantly stirred and heated to 80°C. Next, 20 mL of 0.5 M NaOH solution was added slowly to the solution of the complex. The color of the solution changed immediately from orange to dark brown after addition of NaOH indicating the formation of $MnFe_2O_4$ nanoparticles. The precipitation reaction was then kept at a temperature of about 80°C for 1 h. The product of the GO-MFO nanohybrid was separated from solution by an external magnetic field and washed several times with deionized water and acetone.

Characterization Techniques

The crystalline structure of all samples prepared was analyzed by x-ray diffraction (XRD, Bruker D5005) using CuKα radiation (λ = 0.154 nm) at a step of 0.02° (2θ) at room temperature. The background was subtracted with the linear interpolation method. The chemical groups were analyzed using Fourier Transform Infrared (FTIR) measurements; samples were collected with one layer coating in potassium bromide and compressed into pellets, and spectra in the range of 400 cm^{-1} to 4000 cm^{-1} were recorded with a Nicolet 6700 FT-IR instrument. Transmission electron microscopy (TEM, JEOL-JEM 1010) was conducted to determine the morphology and size distribution of studied samples. The samples for TEM characterization were prepared by placing a drop of a colloidal solution on a carbon-coated copper grid, which was dried at room temperature. Magnetization curves of $MnFe_2O_4$ nanoparticles and GO-$MnFe_2O_4$ nanohybrids were measured by vibrating system magnetometers (VSM, MicroSense, EV9).

Adsorption Studies

Batch experiments were conducted to study adsorption behavior and kinetics process of heavy-metal adsorption. Standard arsenic solution (H_3AsO_4/HNO_3 0,5 M) was prepared at varying concentrations from 0 mg/L to 50 mg/L for generation of the calibration curves for arsenic determination. The concentration of arsenic was measured by using atomic adsorption spectrum (AAS) in accordance with the standard method. The amount of GO, GO-$MnFe_2O_4$ and $MnFe_2O_4$ absorbent materials used for the experiment was fixed at 0.02 gram. The volume of tested arsenic solution was 100 mL. With the GO-MFO sample, the mass ratio of $MnFe_2O_4$:GO used was 7:3 for the study of adsorption.

First, the initial concentration of arsenic was fixed at 30 mg/L, pH was kept at 1–2, the adsorption behavior of samples (GO, MFO and GO-MFO) was investigated at varying adsorption times from 10 min to 90 min. Second, for understanding of adsorption kinetics and determination of maximum adsorption capacity of the nanohybrids, the arsenic solutions of varying concentrations ranging from 10 mg/L to 50 mg/L were prepared and equilibrated time was fixed at 20 min, pH was kept at 1–2. Third, the adsorption property of the nanohybrids was also studied at different pH values (1, 3, 5) of arsenic solution. The solution pH was adjusted by using 1 M NaOH and 1 M HNO_3 as required. Finally, for study of reusability of the nanohybrid sample, the desorption process and removal efficiency of nanohybrids in accordance with adsorption times was evaluated. The pH of water can control the adsorption and desorption capabilities of absorbents. At high pH conditions, the surface functional groups become negatively charged due to deprotonation of the surface functional groups (–OH and –COOH), and; therefore, the adsorbed arsenic species were desorbed.

RESULTS AND DISCUSSION

Formation of $MnFe_2O_4$ Nanoparticles onto the GO Nanosheets

We employed a two-step process for synthesis of the GO-MFO magnetic nanohybrids. The first step was to create the GO nanosheets with oxygen-containing functional groups by using a modified Hummer method. These functionalized groups ensure the good dispersibility and stability of the GO product in aqueous medium.[14] In addition, the functionalized groups introduce more binding sites for anchoring the precursors of metal ions for $MnFe_2O_4$ NPs. In a second step, the MFO NPs were formed on the surface of GO sheets via a co-precipitation reaction of Fe^{+3} and Mn^{+2} ions in the GO solution to produce water-dispersible GO-MFO hybrid materials. The formation of $MnFe_2O_4$ NPs on the surface of GO nanosheets was confirmed using TEM and XRD measurements.

Figure 1a and b display the TEM images of $MnFe_2O_4$ NPs prepared by the co-precipitation method and of GO nanosheets prepared by the modified Hummer method. Figure 1a shows a TEM image of the $MnFe_2O_4$ NPs; the agglomeration of the $MnFe_2O_4$ NPs was observed through TEM analysis. It can be also seen from Fig. 1b that the GO sheets are transparent, and the observation of wrinkles of the GO sheets indicates the GO sheets are thin. Figure 1c and d show the TEM images of GO-MFO nanohybrids at different magnifications. It can be seen that the $MnFe_2O_4$ NPs were anchored on the surface of GO nanosheets; the stable attachment was confirmed even after the ultrasonication step for dispersion of GO-MFO nanohybrids in TEM measurements. The coverage amounts of $MnFe_2O_4$ loaded on the GO sheets were tuned by varying mass ratios of $MnFe_2O_4$ to GO. It was noted that the presence of GO sheets helped to prevent $MnFe_2O_4$ NPs from agglomeration and enabled a good dispersion of these hybrids in an aqueous medium.

The XRD analysis was also employed to confirm the crystalline nature of samples. The XRD patterns of GO sheets, $MnFe_2O_4$ NPs and GO-$MnFe_2O_4$ nanohybrids samples are displayed in Fig. 2. It can be seen from Fig. 2a that for the pristine GO

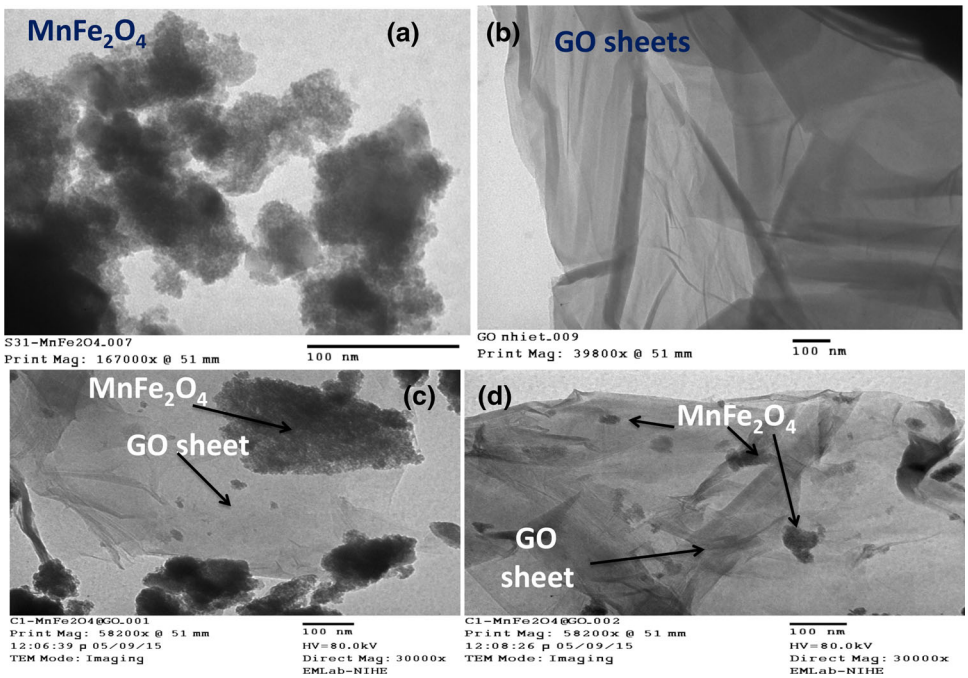

Fig. 1. TEM images of (a) $MnFe_2O_4$ NPs, (b) GO sheets, and (c,d) GO–$MnFe_2O_4$ nanohybrids at different magnifications.

sample, the diffraction peak was found at 10.9° corresponding to the (002) inter-layer spacing of 0.81 nm, indicating the ordinal structures of graphite were exploited, and the oxygen-containing functional groups were inserted into the interspaces.[13,14] For the case of $MnFe_2O_4$ NPs, as shown in Fig. 2b, the XRD pattern exhibits seven characteristic peaks at $2\theta = 18.9°$, 29.7°, 34.98°, 36.5°, 42.52°, 56.19° and 61.96°, indexed as (111), (220), (311), (222), (400), (511) and (440), respectively. These peaks are similar to those from JCPDS 10-0319 for a cubic spinel ferrite structure of $MnFe_2O_4$. The XRD pattern of the GO-MFO sample (see Fig. 2c) shows no other peaks or spectra of impurities, indicating the presence of a pure cubic phase and inverse spinel structure of $MnFe_2O_4$. This result confirmed that $MnFe_2O_4$ NPs were coated on the GO nanosheets.

The obtained TEM and XRD results suggest that the $MnFe_2O_4$ NPs were successfully attached to the surface of GO sheets using a modified coprecipitation process. A fundamental reaction for formation of $MnFe_2O_4$ NPs can be understood as follows[15,16]:

$$MnCl_2 + 2FeCl_3 + 8NaOH \rightarrow MnFe_2O_4 + 8NaCl + 4H_2O \quad (1)$$

Our experimental results revealed that, in the coprecipitation reaction, the particles sizes and shapes of $MnFe_2O_4$ nanocrystals were strongly dependent on synthesis conditions such as the mol ratio of Fe^{2+}/Mn^{3+}, concentration of sodium hydroxide, and pH of the solution. By optimizing experimental conditions, we successfully synthesized the

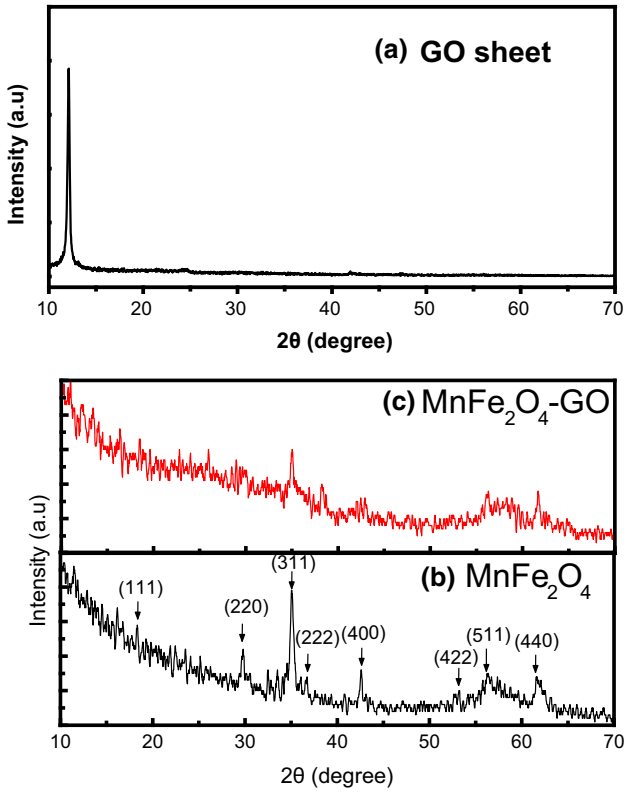

Fig. 2. XRD patterns of (a) GO sheets and (b) $MnFe_2O_4$ NPs and (c) GO-$MnFe_2O_4$ nanohybrids with mass ratio fixed at 3:7, respectively.

$MnFe_2O_4$ NPs with average particle size ~12–15 nm (using Scherrer expression) decorated on the GO sheets.

Magnetic and Surface Interaction Characterizations of GO-$MnFe_2O_4$ Nanohybrids

First, the magnetic property of $MnFe_2O_4$ NPs and GO-$MnFe_2O_4$ nanohybrids was accessed by VSM measurement. Figure 3 shows the magnetic hysteresis loops of $MnFe_2O_4$ NPs and GO-$MnFe_2O_4$ nanohybrid samples measured at room temperature. It was shown that the $MnFe_2O_4$ NPs and GO-$MnFe_2O_4$ samples exhibited ferromagnetic-like behavior. Our experimental results also indicate that the saturation magnetization values (M_s) of MFO NPs and GO-MFO nanohybrid obtained about 19.8 emu/g and 8.7 emu/g, respectively. It can be clearly seen that the M_s value of the GO–MFO sample was smaller when compared to that of bare MFO NPs, because the $MnFe_2O_4$ NPs were wrapped by GO sheets.[17] Noticeably, these GO-MFO hybrids samples can be easily removed from solutions and recycled by applying an external magnetic field (using a small magnet).

Next, to elucidate the interaction of $MnFe_2O_4$ NPs with the functional groups on the surface of GO sheets, FTIR measurement was recorded and analyzed. Figure 4 shows the FTIR spectra of the GO sheets, MFO NPs, and GO-MFO nanohybrid samples. It can be seen that a broad adsorption band at 3446 cm^{-1} for all the samples corresponds to the normal polymeric O–H stretching vibration of H_2O.[14] The band at 1631 cm^{-1} is associated with stretching of the C=O bond of carboxylic groups, while the absorption peaks at 1384 cm^{-1} and 1058 cm^{-1} correspond to the stretching of epoxide groups, respectively.[14] The absorption peak around 558–590 cm^{-1}, which is only present in the FTIR spectra of MFO NPs and GO-MFO nanohybrids, is a characteristic peak corresponding to the stretching vibration of Fe-Mn-O.[14,16,17] The other peaks at 2364 cm^{-1}, 937 cm^{-1}, 815 cm^{-1}, and 458 cm^{-1} might be related to the O=C=O, O–H, C–H, and metal-O groups, respectively.[18,19]

A noticeable change in intensity of the adsorption bands of the oxygenated functional groups was found in the FTIR spectrum of the GO-MFO nanohybrid. This is the result of the presence of the MFO NPs attached to the surface of the GO nanosheets and the reduction of graphene oxide to graphene ratio during the synthesis process. The variation of stretch adsorption intensity in the case of GO-MFO nanohybrid demonstrates that strong interactions exist between MFO NPs and the remaining functional groups on both basal planes (hydroxyl group OH) and edges (carboxyl group COOH) of the GO sheets through the formation of a coordination bond or through simple electrostatic attraction.[16,17] In addition, the slight shift of the peak corresponding to the stretching vibration of Fe-Mn-O bond in GO-MFO hybrids compared to MFO NPs also indicates that the MFO NPs are bound to the GO surface.

Arsenic Adsorption Analysis of GO-$MnFe_2O_4$ Nanohybrids

The adsorption amount and adsorption rate (percentage removal) are calculated based on the difference in the arsenic concentration in the aqueous solution before and after adsorption, according to the following equations[14,17]:

$$q_e = \frac{(C_0 - C_e) \cdot V}{m} \quad (2)$$

$$E(\%) = \left(1 - \frac{C_e}{C_0}\right) \times 100\%, \quad (3)$$

where q_e is the amount of arsenic (mg/g) absorbed on the adsorbents at equilibrium, E is the arsenic removal efficiency (%) of adsorbents. C_0 and C_e (mg/L) are the initial arsenic concentration and the arsenic concentration at equilibrium, respectively; V (L) is the volume of the arsenic solution; and m (g) is the mass of the adsorbents.

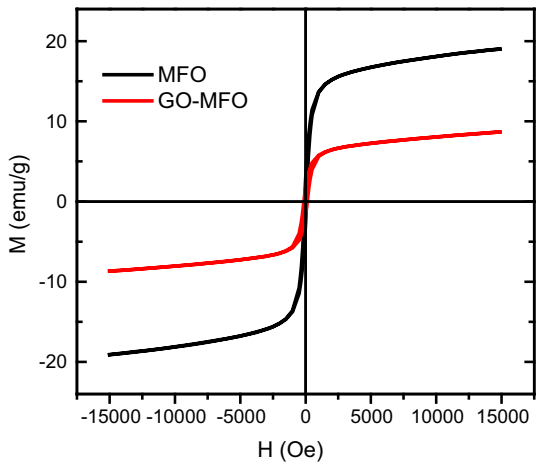

Fig. 3. Magnetic hysteresis loops of the $MnFe_2O_4$ NPs and GO-$MnFe_2O_4$ nanohybrid measured at room temperature.

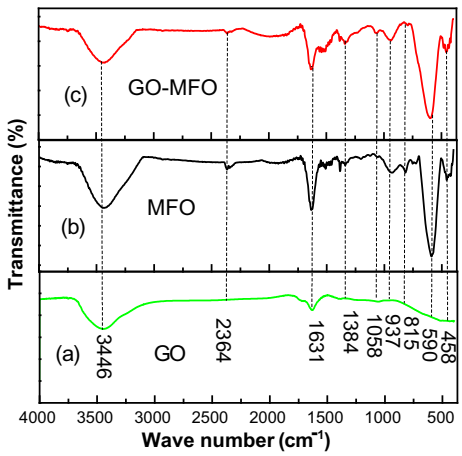

Fig. 4. FTIR spectra of (a) GO sheets, (b) $MnFe_2O_4$ NPs and (c) GO-$MnFe_2O_4$ nanohybrid.

Adsorption Capacity and Removal Efficiency

To analyze the adsorption performance, we studied the adsorption process for three samples (GO, MFO, and GO-MFO) for comparison purposes. First, the adsorption process of all three samples was investigated at different adsorption times from 10 min to 90 min. Figure 5 displays the variation of adsorption capacity of samples as a function of adsorption time. It can be seen from Fig. 5 that the GO-MFO nanohybrid showed better adsorption performances such as a higher adsorption capacity and shorter equilibrium adsorption time as compared with bare MFO NPs and GO sheets. Our experimental results reveal that the adsorption capacities of GO, MFO, and GO-MFO obtained ~40 mg/g, 139.2 mg/g and 149.3 mg/g, respectively. More importantly, the equilibrium adsorption time of GO-MFO was 20 min, which is shorter than that of the MFO sample (40 min) and the GO sample (45 min). Similarly, the removal efficiency of GO-MFO obtained the highest value of 99.9%, which is much higher than that of MFO (90.1%) and GO (27.8%) (see Table I). This result suggests that the GO-MFO nanohybrid has the better adsorption performance than that of bare MFO nanoparticles and GO nanosheets. It was noted that the measured concentrations of arsenic as well as the calculated adsorption capacities and removal efficiency obtained average values for three trials from the AAS measurements. The estimation of error in the AAS measurement is about 5–7%.

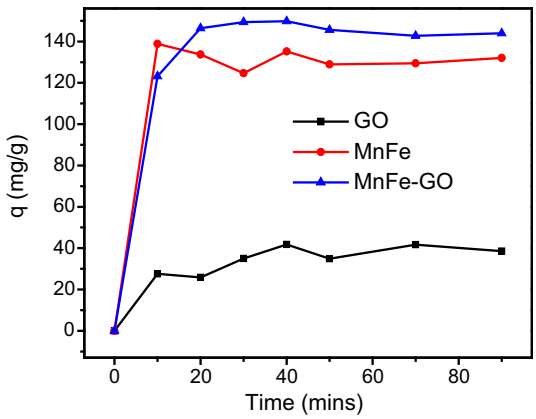

Fig. 5. Variation of adsorption capacity as a function of contact time for investigated samples (GO, MFO, and GO-MFO).

Adsorption Kinetics

In the adsorption experiments, determination of adsorption kinetics is important for understanding of adsorption mechanism of adsorbent materials. In this work, the adsorption kinetics of arsenic by all samples are fit with both pseudo-first-order and pseudo-second-order models.

The pseudo-first-order equation can be described as:

$$\ln(q_e - q_t) = \ln q_e - \frac{k_1 t}{2.303}. \quad (4)$$

The pseudo-second-order equation can be described as:

$$\frac{t}{q_e} = \frac{1}{k_2 q_e^2} + \frac{1}{q_e} t, \quad (5)$$

where k_1 is the rate constant for adsorption (g mg^{-1} min^{-1}), and k_2 is the rate constant for the pseudo-second-order adsorption process.

The fitted results of studied samples were fitted with both pseudo-first-order and pseudo-second-order kinetic models. The results reveal that the pseudo-second-order kinetic model is well fitted. The linear plots of t/q_e versus time showed a good agreement between experimental data and calculated values (see Fig. 6) for different adsorbent materials. The correlation coefficient (R^2) for the pseudo-second-order model had high values >99%. This indicates that the adsorption process complies well with the pseudo-second order model (see Table I).

The data of arsenic adsorption were also fitted with various Langmuir and Freundlich isotherm models (see Table II). First, our data was fitted with the Langmuir isotherm model that assumed that the absorbent surface can only occur at the surface monolayer and adsorption occurs homogeneously. The Langmuir isotherm is expressed as follows:

$$\frac{C_e}{q_e} = \frac{1}{k_L \cdot q_m} + \frac{C_e}{q_m}, \quad (6)$$

where q_e and q_m are the amounts of arsenic (mg/g) absorbed on the adsorbent at the equilibrium and maximum adsorption capacity, C_e is the equilibrium concentration of arsenic in the aqueous solution (mg/L), and k_L is the Langmuir binding constant (L/

Table I. The pseudo-second-order kinetic model was fitted with experimental data

	Pseudo-second–order kinetic model		
Samples	**k_2 (g mg^{-1} min^{-1})**	**R^2**	**E (%)**
GO	0.02419	0.97289	27.8
MFO	0.00764	0.99888	90.1
GO-MFO	0.00692	0.99823	99.9

mg). Plotting C_e/q_e against C_e (see Fig. 7a) gives a straight line wherein the slope and intercept are $1/q_m$ and $1/(k_L q_m)$, respectively. From the slope and intercept, the values of q_m and k_L could be estimated to be 240.385 mg/g and 0.00416 L/mg, respectively, while the correlation coefficient (R^2) value is about 0.978 (see Table III).

Next, our data was fitted with the Freundlich isotherm model, which describes the multilayer adsorption of adsorbate on a heterogeneous adsorbent surface. The Freundlich isotherm is represented by the following equation:

$$\ln q_e = \ln k_f + \frac{1}{n} \cdot \ln C_e, \quad (7)$$

where the C_e is the equilibrium concentration of arsenic in solution (mg/L), q_e is the amount of arsenic (mg/g) absorbed on the adsorbent at the equilibrium adsorption capacity. The k_f is the Freundlich binding constant (L/mg) and $1/n$ is a constant related to the surface heterogeneity. Plotting Ln(q_e) against Ln(C_e) (see Fig. 7b) gives a straight line wherein the slope and intercept are $1/n$ and ln(k_f), respectively. The correlation coefficient (R^2) value is about 0.988.

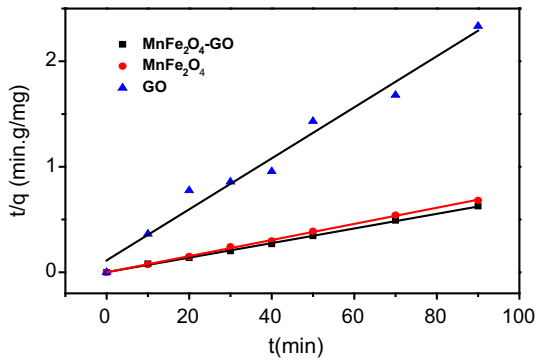

Fig. 6. The pseudo-second-order kinetic plot for adsorption kinetics of arsenic for different adsorbents.

Effect of pH Value on Adsorption Process

One of the most important factors affecting the capacity of adsorbent in wastewater treatment is the pH value of solution. The control of pH is very important for the adsorption process, because the pH affects not only the surface charge of adsorbent, but also the degree of ionization and the speciation of the adsorbate during the reaction.[20–22] In this work, the effect of pH on the adsorption process was tested with three values of pH = 1, 3, and 5. Our results indicate that the adsorption capacity of

Table II. The Langmuir and Freundlich isotherm data for arsenic adsorption on the GO-$MnFe_2O_4$ magnetic nanohybrid

Concentration (ppm)	m (g)	V_{As} (mL)	C_e (mg/L)	q_e (mg/g)	C_e/q_e (mg/g)	ln C_e	ln q_e
10	0.02	100	0.846	45.096	0.0187	−0.167	3.809
20	0.02	100	2.822	85.880	0.0328	1.037	4.453
30	0.02	100	5.3672	123.157	0.0435	1.680	4.813
40	0.02	100	7.864	158.293	0.0496	2.062	5.064
50	0.02	100	13.57	182.148	0.0745	2.608	5.205

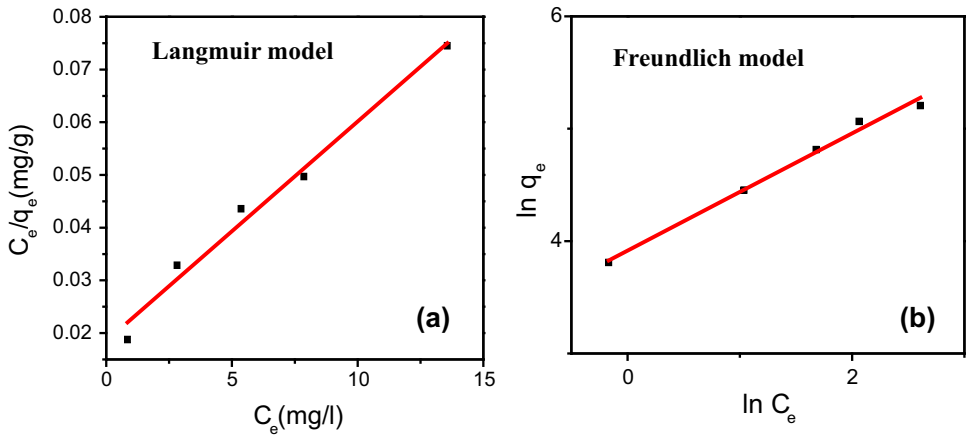

Fig. 7. The experimental data were fitted with Langmuir and Freundlich isotherm models for the arsenic adsorption on GO-$MnFe_2O_4$ nanohybrids at T = 25°C, pH = 1–2, m = 0.02 g and time = 20 min.

Table III. Adsorption constants and correlation coefficient (R^2) for arsenic adsorption fitting with various isotherm models

Langmuir model			Freundlich model		
k_L (L/mg)	q_m (mg/g)	R^2	n	k_f (mg/g)	R^2
0.00416	240.385	0.978	1.917	50.169	0.988

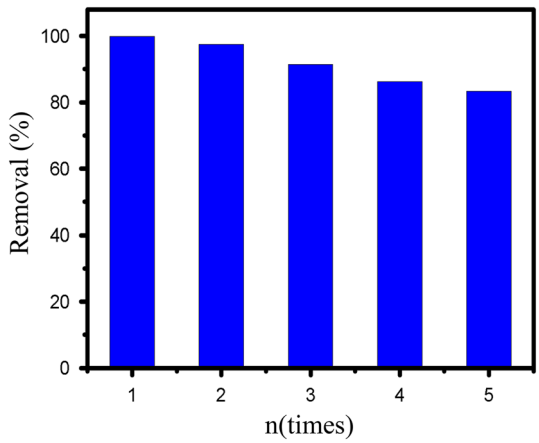

Fig. 8. Reusability function of GO-MFO nanohybrid adsorbent.

nanohybrid decreases with an increase of pH value. The effect of solution pH on the adsorption can be understood as follows: there are a large number of functional groups –OH and –COOH on the surface of MFO nanoparticles as well as GO sheets. At low pH conditions, the number of H ions in the solution increases and –OH and –COOH groups becomes positively charged $–OH_2^+$ and $–COOH_2^+$, increasing the adsorption capacity of negative arsenic ions on the surface of the adsorbent. At higher pH values, –OH and –COOH groups are ionized to $–O^-$ and $–COO^-$, decreasing the adsorption of arsenic.[17]

$$\text{MFO-OH}_2^+ + \text{H}_3\text{AsO}_4^- \rightarrow \text{MFO-OH}_2^+ - \text{H}_3\text{AsO}_4^- \quad (8)$$

$$\text{GO-COOH}_2^+ + \text{H}_3\text{AsO}_4^- \rightarrow \text{GO-COOH}_2^+ - \text{H}_3\text{AsO}_4^- \quad (9)$$

Desorption Studies and Reusability of Adsorbent Material

We also studied desorption of arsenic substance from the surface of the adsorbent. The desorption process of arsenic was conducted by tuning the pH value of the solution with use of 1 M NaOH. It revealed that >98% of adsorbed arsenic was released from the GO-MFO adsorbent. Next, we used the same sample and evaluated the reusability of the sample for adsorption times. Figure 8 shows the variation of removal efficiency of the nanohybrid sample with adsorption times. The removal efficiency for the first time ~99.9% decreases to 83.6% for the fifth time. Our results suggested that the GO-MFO can be reused over 5 times.

CONCLUSIONS

In this work, the magnetic nanohybrid GO-MFO was synthesized by a two-step process of the Hummers method and the coprecipitation method. The MFO nanoparticles with average sizes ~12–15 nm were formed and stably anchored on the surface of GO sheets. We demonstrated a high potential for application of a GO-MFO nanohybrid used for a magnetically separable adsorbent for highly efficient arsenic removal from water. The GO-MFO material displayed better adsorption quality than that of bare MFO nanoparticles and GO sheets. The kinetic studies revealed that the adsorption process of GO-MFO was fitted well with a pseudo-second-order kinetic equation and the Freundlich isotherm model.

ACKNOWLEDGEMENTS

This research is funded by the Vietnam National Foundation for Science and Technology Development (NAFOSTED) under grant number 103.02-2015.20. One of the authors (V.N. Phan) would like to acknowledge the partial support from the Vietnam's Ministry of Education and Training (MOET) through a project with code B2014-01-73.

REFERENCES

1. M. Jakariya and M.S. Deeble, Evaluation of Arsenic Mitigation in Four Countries of the Greater Mekong Region—Final Report, UNICEF-AusAID (2008).
2. T. Agusa, P.T.K. Trang, V.M. Lan, D.H. Anh, S. Tanabe, P.H. Viet, and M. Berg, *Sci. Total Environ.* 562, 488 (2014).
3. P. Xu, G.M. Zeng, D.L. Huang, C.L. Feng, S. Huc, M.H. Zhao, C. Lai, Z. Wei, C. Huang, G.X. Xie, and Z.F. Liu, *Sci. Total Environ.* 424, 1 (2012).
4. S.R. Chowdhury and E.K. Yanful, *J. Environ. Manag.* 91, 2238 (2010).
5. G.C. Silva, F.S. Almeida, A.M. Ferreira, and V.S.T. Ciminelli, *Mater. Res.* 15, 403 (2012).
6. K.S. Novoselov, A.K. Geim, S.V. Morozov, D. Jiang, Y. Zhang, S.V. Dubonos, I.V. Grigorieva, and A.A. Firsov, *Science* 306, 666 (2004).
7. A.K. Geim and K.S. Novoselov, *Nat. Mater.* 6, 183 (2007).
8. J.H. Deng, X.R. Zhang, G.M. Zeng, J.L. Gong, Q.Y. Niu, and J. Liang, *Chem. Eng. J.* 226, 189 (2013).
9. H. Wang, X. Yuan, Y. Wu, X. Chen, L. Leng, H. Wang, H. Li, and G. Zeng, *Chem. Eng. J.* 262, 597 (2015).
10. J. Li, S. Zhang, C. Chen, G. Zhao, X. Yang, J. Li, and X. Wang, *ACS Appl. Mater. Interfaces* 4, 4991 (2012).

11. G. Gollavelli, C.C. Chang, and Y.C. Ling, *ACS Sustain. Chem. Eng.* 1, 462 (2013).
12. S. Zhan, D. Zhu, S. Ma, W. Yu, Y. Jia, Y. Li, H. Yu, and Z. Shen, *ACS Appl. Mater. Interfaces* 7, 4290 (2015).
13. N.T. Lan, D.T. Chi, N.X. Dinh, N.D. Hung, H. Lan, P.A. Tuan, L.H. Thang, N.N. Trung, N.Q. Hoa, T.Q. Huy, N.V. Quy, D.T. Tung, V.N. Phan, and A.T. Le, *J. Alloy. Comp.* 615, 843 (2014).
14. P.T.L. Huong, N.T. Huyen, C.D. Giang, N. Tu, V.N. Phan, N.V. Quy, T.Q. Huy, D.T.M. Hue, H.D. Chinh, and A.T. Le, *J. Nanosci. Nanotechnol.* (2015). doi:10.1166/jnn.2016.12161.
15. J. Shen, Y. Hu, M. Shi, N. Li, H. Ma, and M. Ye, *J. Phys. Chem.* 114, 1498 (2010).
16. S. Chella, P. Kollu, E.V.P.R. Komarala, S. Doshi, M. Saranya, S. Felix, R. Ramachandran, P. Saravanan, V.L. Koneru, V. Venugopal, S.K. Jeong, and A.N. Grace, *Appl. Sur. Sci.* 327, 27 (2015).
17. S. Kumar, R.R. Nair, P.B. Pillai, S.N. Gupta, M.A.R. Iyengar, A.K. Sood, and A.C.S. Appl, *Mater. Interfaces* 6, 17526 (2014).
18. Z. Guo, M.V. Reddy, B.M. Goh, A.K.P. San, Q. Bao, and K.P. Loh, *RSC Adv.* 3, 19051 (2013).
19. T. Remyamol, P. Gopinath, and H. John, *RSC Adv.* 4, 29901 (2014).
20. Z. Wu, W. Li, P.A. Webley, and D. Zhao, *Adv. Mater.* 24, 485 (2012).
21. V. Chandra, J. Park, Y. Chun, J.W. Lee, I. Hwang, and K.S. Kim, *ACS Nano* 4, 3979 (2010).
22. X. Luo, C. Wanga, S. Luo, R. Dong, X. Tua, and G. Zeng, *Chem. Eng. J.* 187, 45 (2012).